

Quantum circuits for the realization of equivalent forms of one-dimensional discrete-time quantum walks on near-term quantum hardware

Shivani Singh,^{1,2} C. Huerta Alderete^{3,4}, Radhakrishnan Balu,^{5,6}
Christopher Monroe,³ Norbert M. Linke,³ and C. M. Chandrashekar^{1,2}

¹*The Institute of Mathematical Sciences, C. I. T. Campus, Taramani, Chennai 600113, India*

²*Homi Bhabha National Institute, Training School Complex, Anushakti Nagar, Mumbai 400094, India*

³*Joint Quantum Institute, Department of Physics and Joint Center for Quantum Information and Computer Science, University of Maryland, College Park, Maryland 20742, USA*

⁴*Instituto Nacional de Astrofísica, Óptica y Electrónica, Calle Luis Enrique Erro No. 1, Santa María Tonantzintla, Puebla Codigo Postal 72840, Mexico*

⁵*Computational and Information Sciences Directorate, U.S. Army Research Laboratory, Adelphi, Maryland 20783, USA*

⁶*Department of Mathematics and Norbert Wiener Center for Harmonic Analysis and Applications, University of Maryland, College Park, Maryland 20742, USA*



(Received 11 February 2020; accepted 12 November 2021; published 1 December 2021)

Quantum walks are a promising framework for developing quantum algorithms and quantum simulations. They represent an important test case for the application of quantum computers. Here we present different forms of discrete-time quantum walks (DTQWs) and show their equivalence for physical realizations. Using an appropriate digital mapping of the position space on which a walker evolves to the multiqubit states of a quantum processor, we present different configurations of quantum circuits for the implementation of DTQWs in one-dimensional position space. We provide example circuits for a five-qubit processor and address scalability to higher dimensions as well as larger quantum processors.

DOI: [10.1103/PhysRevA.104.062401](https://doi.org/10.1103/PhysRevA.104.062401)

I. INTRODUCTION

There is great interest in developing quantum algorithms for potential speedups over conventional computers, and progress is being made in mapping such algorithms to current technology [1,2]. Device architecture, qubit connectivity, gate fidelity, and qubit coherence time are metrics that define the trade-off in designing device-specific circuits. Quantum walks [3,4], exploiting quantum superposition of multiple paths, have played an important role in the development of a wide variety of quantum algorithms. Examples include algorithms for quantum search [5–9], graph isomorphism problems [10–12], ranking nodes in a network [13–16], and quantum simulation at low- and high-energy scales [17–26].

There are two main variants of quantum walks, the discrete-time quantum walk (DTQW) [27,28] and the continuous-time quantum walk (CTQW) [29,30]. The DTQW is defined on a Hilbert space comprising internal states of the single particle called coin space and position space, with the evolution being driven by a position shift operator controlled by a quantum coin operator. The CTQW is defined directly on the position Hilbert space, with the evolution being driven by the Hamiltonian of the system and adjacency matrix of the position space. In both variants, the probability distribution of the particle spreads quadratically faster in position space compared to the classical random walk [5,31–34].

Due to the Hilbert space configuration of DTQWs one can define many different forms of quantum coin operators

and position shift operators that control the dynamics leading to variants such as the standard DTQW, directed DTQW [35–37], split-step DTQW [38–40], and the Szegedy walk [41]. These models have been successfully used to mimic different quantum phenomena such as Dirac cellular automata [40,42,43], strong and weak localizations [44,45], topological phases [46,47], and many more.

Experimental implementations of quantum walks have been reported in cold atoms [48,49], NMR systems [50,51], and photonic systems [52–56]. DTQW implementations are ideally suited for lattice-based quantum systems in which the lattice site represents the position space. The DTQW is realized on an ion-trap system by mapping the position space to the motional phase space [57,58]. However, implementation of quantum walks on the quantum circuit is crucial to explore the practical realm of their algorithmic applications. The quantum-circuit-based implementation of DTQWs was first performed on a multiqubit NMR system [51]. On any hardware, limitations in the qubit number and coherence time restrict the number of steps that can be implemented. For implementation of a DTQW on a quantum circuit, one needs to map the position state to the multiqubit state. Protocols using one such mapping on an $(N + 1)$ -qubit superconducting system to implement N steps of a DTQW was reported [59]. Recently, an optimal form of the quantum circuit for the realization of a DTQW on a five-qubit ion-trap quantum processor was presented and used for digital simulation of Dirac cellular automata [60]. Here we present a complete theory beyond

the optimal form of quantum circuits that was used for the realization of Dirac cellular automata.

In this paper, we review different forms of DTQWs and show their equivalence concerning physical implementation on a quantum circuit. We also present various forms of quantum circuits that can be realized on a five-qubit quantum processor for the implementation of one-dimensional DTQWs. The circuits provided are for two variants of the DTQW, a standard QW and a directed QW, that can be used to realize other forms of the DTQW and Dirac cellular automata. They can be further scaled up and generalized to implement multiparticle DTQWs and DTQW-based algorithms.

II. VARIANTS OF DTQWs AND THEIR EQUIVALENCE

A. Different forms of DTQWs

A DTQW is defined by the combination of particle (coin) and position Hilbert space $\mathcal{H} = \mathcal{H}_c \otimes \mathcal{H}_p$. The coin Hilbert space is defined by the particles' internal states $\mathcal{H}_c = \text{span}\{|\uparrow\rangle, |\downarrow\rangle\}$, and the one-dimensional position Hilbert space is spanned by $\mathcal{H}_p = \text{span}\{|x\rangle\}$, where $x \in \mathbb{Z}$ represents the labels on the position states. The generic initial state of the particle $|\psi\rangle_c$ can be written as

$$|\psi(\delta, \eta)\rangle_c = \cos(\delta)|\uparrow\rangle + e^{-i\eta} \sin(\delta)|\downarrow\rangle. \quad (1)$$

Each step of the walk evolves using a quantum coin operator acting on the particle space followed by a conditioned position shift operator acting on the entire Hilbert space. By modifying the coin and shift operators, different forms of DTQWs are achieved. The variants can have the same coin operation but have different shift operations. The coin operator with a single parameter is given by a rotation operator,

$$\hat{C}(\theta) = \begin{bmatrix} \cos(\theta) & -i \sin(\theta) \\ -i \sin(\theta) & \cos(\theta) \end{bmatrix} \otimes \mathcal{I}_l. \quad (2)$$

Here \mathcal{I}_l is the identity operator in the position space of length l .

Standard DTQW (SQW). Each step of a SQW is realized by applying the operator $\hat{W} = \hat{S}\hat{C}(\theta)$, where the coin operation for the SQW is given by Eq. (2) and the conditioned position shift operator \hat{S} is given by

$$\hat{S} = \sum_{x \in \mathbb{Z}} (|\uparrow\rangle\langle\uparrow| \otimes |x-1\rangle\langle x| + |\downarrow\rangle\langle\downarrow| \otimes |x+1\rangle\langle x|). \quad (3)$$

The state of the particle in extended position space after t steps of a SQW is given by

$$|\Psi(t)\rangle = \hat{W}^t [|\psi\rangle_c \otimes |x=0\rangle] = \sum_{x=-t}^t \begin{bmatrix} \psi_{x,t}^\uparrow \\ \psi_{x,t}^\downarrow \end{bmatrix}. \quad (4)$$

The probability of finding the particle at position and time (x, t) is

$$P(x, t) = \|\psi_{x,t}^\uparrow\|^2 + \|\psi_{x,t}^\downarrow\|^2. \quad (5)$$

Figure 1 shows the probability distribution of a SQW for different initial states for $\theta = \pi/4$. The symmetry of the probability distribution naturally depends on the particular choice

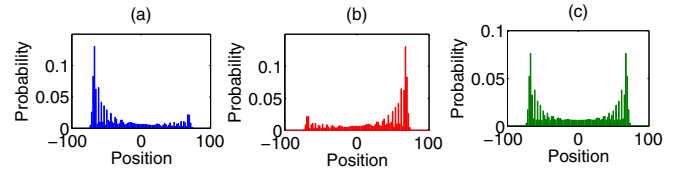


FIG. 1. Probability distribution after 100 time steps of a standard DTQW (SQW) for different initial states with the coin parameter $\theta = \pi/4$. Initial states are $|\Psi_{\text{in}}\rangle = |\uparrow\rangle \otimes |x=0\rangle$ for (a), $|\Psi_{\text{in}}\rangle = |\downarrow\rangle \otimes |x=0\rangle$ for (b), and $|\Psi_{\text{in}}\rangle = \frac{1}{\sqrt{2}}(|\uparrow\rangle + |\downarrow\rangle) \otimes |x=0\rangle$ for (c). Alternate sites will have zero probability in a SQW irrespective of the initial state.

of the initial state of the walker. The symmetry and variance of the final distribution can also be affected by adding phases and thus taking advantage of the entire Bloch sphere for the coin operation in Eq. (2) [61].

Directed DTQW (DQW). In one-dimensional position space each step of the DQW is evolved by applying the coin operation as given by Eq. (2) in coin space followed by a position shift operator \hat{S}_d of the form

$$\hat{S}_d = \sum_{x \in \mathbb{Z}} (|\uparrow\rangle\langle\uparrow| \otimes |x\rangle\langle x| + |\downarrow\rangle\langle\downarrow| \otimes |x+1\rangle\langle x|). \quad (6)$$

The shift operator at time t retains the particle at the existing position state or translates to the right conditioned on the internal state of the particle. Each step of the walk is realized by applying the operator $\hat{W}_d = \hat{S}_d\hat{C}(\theta)$. When the particle is in the superposition of the internal state, during each step of the walk, some amplitude of the particle will simultaneously remain at the existing position state and translate to the right position state. In DQWs, the probability amplitude is spread over half the size of the position space compared to the spread of SQW.

Split-step DTQW (SSQW). In this variant, each step of the walk is a composition of two half-step evolutions,

$$\hat{W}_{ss} = \hat{S}_+ \hat{C}(\theta) \hat{S}_- \hat{C}(\theta). \quad (7)$$

The single-parameter coin operator is again given by Eq. (2), and the two shift operators have the forms

$$\hat{S}_- = \sum_{x \in \mathbb{Z}} (|\uparrow\rangle\langle\uparrow| \otimes |x-1\rangle\langle x| + |\downarrow\rangle\langle\downarrow| \otimes |x\rangle\langle x|), \quad (8a)$$

$$\hat{S}_+ = \sum_{x \in \mathbb{Z}} (|\uparrow\rangle\langle\uparrow| \otimes |x\rangle\langle x| + |\downarrow\rangle\langle\downarrow| \otimes |x+1\rangle\langle x|). \quad (8b)$$

During each step of the SSQW, the particle remains in the same position and also moves to the left and right positions conditioned on the internal state of the particle. This leads to a probability distribution that is different from the SQW. In addition to that, a different value of θ can be used for each half step, giving additional control over the dynamics and probability distribution.

In Fig. 2 we show the probability distribution over position space after 100 steps of a SQW, DQW, and SSQW. The position space explored in the DQW is half the size of the SQW. The probability of finding the particle in each position space is nonzero for the DQW when compared to the SQW, in which the probability of finding the particle at every alternate position is zero. Although the size of the position space is

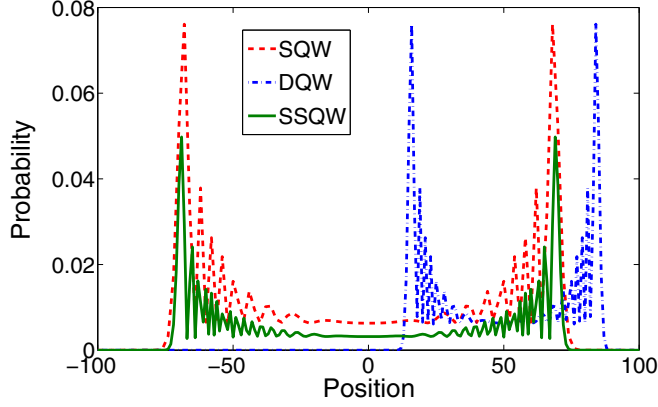


FIG. 2. Probability distribution for standard DTQW (SQW), directed DTQW (DQW), and a split-step quantum walk (SSQW) with the coin parameter $\theta = \pi/4$ after 100 steps. In the plot, the zero-probability values at alternate positions are discarded from the SQW. The spread in position space for the SQW and SSQW are identical, but the peak values of the distribution are different. The spread is different for SQW and DQW, but their peak values are identical. The initial state is $|\Psi_{\text{in}}\rangle = \frac{1}{\sqrt{2}}(|\uparrow\rangle + |\downarrow\rangle) \otimes |x=0\rangle$ for all cases.

the same for both SSQW and SQW, a nonzero probability of finding the particle at all positions is seen in the SSQW compared to the SQW, resulting in correspondingly lower peak values.

B. Equivalence of variants of discrete-time quantum walk

Among the three forms of the walk presented above, the SSQW comprises both features, extended position states and nonzero probability at all positions. Therefore, one can consider SSQWs to be the most general form of a DTQW evolution. The state at any position x and time $(t+1)$ after the operation of \hat{W}_{ss} at time t will be $\psi_{x,t+1} = \psi_{x,t+1}^{\uparrow} + \psi_{x,t+1}^{\downarrow}$, where

$$\psi_{x,t+1}^{\uparrow} = \cos(\theta)[\cos(\theta)\psi_{x+1,t}^{\uparrow} - i\sin(\theta)\psi_{x+1,t}^{\downarrow}] - i\sin(\theta)[-i\sin(\theta)\psi_{x,t}^{\uparrow} + \cos(\theta)\psi_{x,t}^{\downarrow}], \quad (9a)$$

$$\psi_{x,t+1}^{\downarrow} = -i\sin(\theta)[\cos(\theta)\psi_{x,t}^{\uparrow} - i\sin(\theta)\psi_{x,t}^{\downarrow}] + \cos(\theta)[-i\sin(\theta)\psi_{x-1,t}^{\uparrow} + \cos(\theta)\psi_{x-1,t}^{\downarrow}]. \quad (9b)$$

In the description below, we show that the amplitudes of the walker positions in the different quantum walk variants are identical after relabeling of the position state, which establishes that they are all equivalent.

Equivalence of the SQW and SSQW. If we evolve two steps of the SQW we will arrive at a state that is identical to Eq. (9) with only a replacement of $|x \pm 1\rangle$ with $|x \pm 2\rangle$. Without loss of generality we can show that

$$\hat{W}_{ss} \equiv \hat{W}^2, \quad \hat{S}_+ \hat{C}(\theta) \hat{S}_- \hat{C}(\theta) \equiv [\hat{S} \hat{C}(\theta)]^2, \quad (10)$$

where

$$\begin{aligned} \hat{W}_{ss} &= \hat{S}_+ \hat{C}(\theta) \hat{S}_- \hat{C}(\theta) \\ &= [(\cos^2 \theta |\uparrow\rangle\langle\uparrow| - i\sin \theta \cos \theta |\uparrow\rangle\langle\downarrow|) \otimes \sum |x-1\rangle\langle x| + (-i\sin \theta \cos \theta |\downarrow\rangle\langle\uparrow| - \sin^2 \theta |\downarrow\rangle\langle\downarrow|) \otimes \sum |x\rangle\langle x| \\ &\quad + (-\sin^2 \theta |\uparrow\rangle\langle\uparrow| - i\sin \theta \cos \theta |\uparrow\rangle\langle\downarrow|) \otimes \sum |x\rangle\langle x| + (-i\sin \theta \cos \theta |\downarrow\rangle\langle\uparrow| + \cos^2 \theta |\downarrow\rangle\langle\downarrow|) \otimes \sum |x+1\rangle\langle x|] \end{aligned} \quad (11)$$

and

$$\begin{aligned} \hat{W}^2 &= \hat{S} \hat{C}(\theta) \hat{S} \hat{C}(\theta) \\ &= [(\cos^2 \theta |\uparrow\rangle\langle\uparrow| - i\sin \theta \cos \theta |\uparrow\rangle\langle\downarrow|) \otimes \sum |x-2\rangle\langle x| + (-i\sin \theta \cos \theta |\downarrow\rangle\langle\uparrow| - \sin^2 \theta |\downarrow\rangle\langle\downarrow|) \otimes \sum |x\rangle\langle x| \\ &\quad + (-\sin^2 \theta |\uparrow\rangle\langle\uparrow| - i\sin \theta \cos \theta |\uparrow\rangle\langle\downarrow|) \otimes \sum |x\rangle\langle x| + (-i\sin \theta \cos \theta |\downarrow\rangle\langle\uparrow| + \cos^2 \theta |\downarrow\rangle\langle\downarrow|) \otimes \sum |x+2\rangle\langle x|]. \end{aligned} \quad (12)$$

The equivalence shown in Eq. (10) can be established by mapping position space $|x \pm 2\rangle$ to $|x \pm 1\rangle$. The equivalence of Eqs. (11) and (12) can also be obtained by using a modified version of the shift operators S'_- and S'_+ in which $|x \pm 1\rangle$ in S_- and S_+ [Eq. (8)] is replaced with $|x \pm 2\rangle$. That is,

$$\hat{W}'_{ss} = \hat{S}'_+ \hat{C}(\theta) \hat{S}'_- \hat{C}(\theta) = [\hat{S} \hat{C}(\theta)]^2. \quad (13)$$

Since the operator $\hat{W}_{ss} \equiv \hat{W}'_{ss} = [\hat{S} \hat{C}(\theta)]^2$, the equivalence shown in Eq. (10) can be established, and all three operators will execute an identical transformation when applied to any initial state.

Equivalence of the SQW and DQW. Two SQW steps are equivalent to two DQW steps followed by a translation operator which executes a global shift on the position space. For the choice of shift operator that we have used, along with directed

translation we can show that

$$\hat{W}^2 \equiv \hat{T}_- \hat{W}_d^2, \quad [\hat{S} \hat{C}(\theta)]^2 \equiv \hat{T}_- [\hat{S}_d \hat{C}(\theta)]^2, \quad (14)$$

where the forms of $\hat{C}(\theta)$, \hat{S} , and \hat{S}_d are given in Eqs. (2), (3), and (6), respectively, and $\hat{T}_- = (\mathcal{I}_c \otimes \sum |x-1\rangle\langle x|)$. This can be explicitly shown by expanding the operators; \hat{W}^2 is given in Eq. (12), and

$$\begin{aligned} \hat{W}_{TD} &= \hat{T}_- \hat{W}_d^2 \\ &= \hat{T}_- [\hat{S}_d \hat{C}(\theta) \hat{S}_d \hat{C}(\theta)] \\ &= [(\cos^2 \theta |\uparrow\rangle\langle\uparrow| - i\sin \theta \cos \theta |\uparrow\rangle\langle\downarrow|) \otimes \sum |x-1\rangle\langle x| \\ &\quad + (-i\sin \theta \cos \theta |\downarrow\rangle\langle\uparrow| - \sin^2 \theta |\downarrow\rangle\langle\downarrow|) \otimes \sum |x\rangle\langle x| \end{aligned}$$

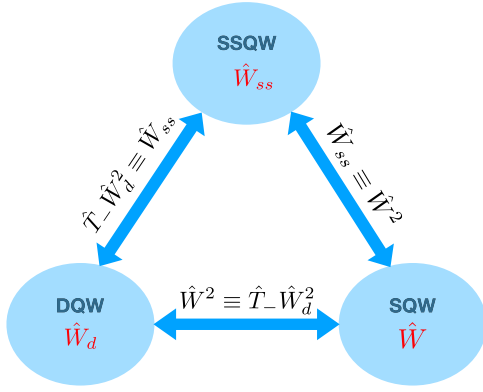


FIG. 3. Systematic presentation of the equivalence of the three forms of DTQWs.

$$\begin{aligned}
 &+ (-\sin^2 \theta |\uparrow\rangle\langle\uparrow| - i \sin \theta \cos \theta |\uparrow\rangle\langle\downarrow|) \otimes \sum |x\rangle\langle x| \\
 &+ (-i \sin \theta \cos \theta |\uparrow\rangle\langle\downarrow| + \cos^2 \theta |\downarrow\rangle\langle\downarrow|) \\
 &\otimes \sum |x+1\rangle\langle x|. \quad (15)
 \end{aligned}$$

By replacing $x \pm 2$ with $x \pm 1$ in Eq. (12) we can show that $\hat{W}_{TD} \equiv \hat{W}^2$. Therefore, for all physical realizations mapping the position space of the walker onto multiqubit states of a quantum processor, one can ignore the alternate positions with zero probability in the SQW. A resulting probability distribution is equivalent to the translated DQW.

Equivalence of the SSQW and DQW. A SSQW as described by the operator \hat{W}_{ss} is equal to two DQW steps described by \hat{W}_d followed by a global translation operator of the form $\hat{T}_- = (\mathcal{I}_c \otimes \sum |x-1\rangle\langle x|)$. The probability distribution of $2t$ time steps of the directed walk is the same as the probability distribution of t steps of the split-step walk, i.e.,

$$\hat{W}_{ss} = \hat{T}_- \hat{W}_d^2, \quad (16)$$

where \hat{W}_{ss} and \hat{W}_d are given in Eqs. (7) and (6), respectively. $\hat{T}_- \hat{W}_d^2$ is given in Eq. (15). Therefore, from Eqs. (10), (14), and (16) we get

$$\hat{W}_{ss} = \hat{T}_- \hat{W}_d^2 \equiv \hat{W}^2. \quad (17)$$

This implies that $\psi_{x\pm 1}^{\uparrow(\downarrow)} = 0$, i.e., the position with zero probability in the SQW. Thus, by discarding the positions with zero probability and relabeling values of position $x \pm 2$ as values of $x \pm 1$, the two-step SQW is equivalent to the SSQW [62].

A schematic representation of the equivalence of all three forms of DTQWs is shown in Fig. 3, while Fig. 4 shows the probability distribution comparison for all three forms of DTQWs. The probability distribution of the SSQW is equivalent to half of the time evolution of the SQW and DQW. The probability values are the same for all three forms. Translation of the DQW in position space recovers the SSQW, and discarding of position space with zero probability in the SQW reduces its spread in position space and recovers the SSQW.

Therefore, a quantum circuit which can implement one form of the DTQW is sufficient to recover the exact probability distribution of the others by relabeling the position state associated with the multiqubit state on the processor.

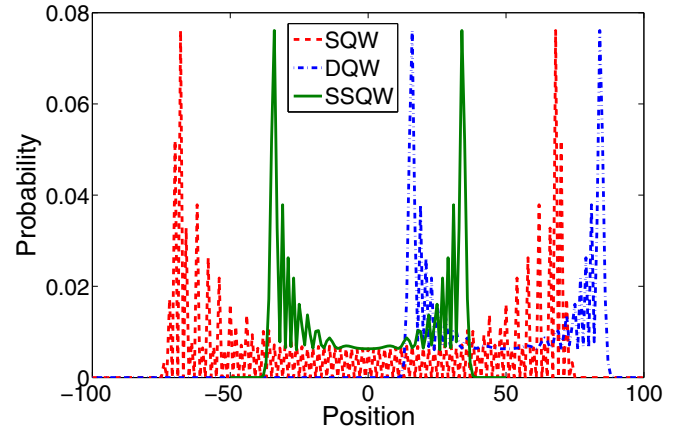


FIG. 4. Equivalence of the probability distribution for different forms of DTQWs, i.e., the SQW and DQW for 100 steps and the SSQW for 50 steps, with the coin parameter $\theta = \pi/4$. Alternate sites of the SQW have zero probability, and thus 100 steps of SQW are equivalent to 50 time steps of the SSQW. The initial state is $|\Psi_{in}\rangle = \frac{1}{\sqrt{2}}(|\uparrow\rangle + |\downarrow\rangle) \otimes |x=0\rangle$.

III. QUANTUM CIRCUIT FOR IMPLEMENTING THE DTQW

To implement the DTQW on a quantum circuit in a one-dimensional position Hilbert space of size 2^N , $(N+1)$ qubits are needed. Among $(N+1)$ qubits, one qubit acts as the coin, and the states of the remaining qubits are mapped to the position states in the DTQW. The basis for each qubit is characterized by its internal states, $|0\rangle$ and $|1\rangle$. In principle, in 2^N position space, $(2^{N-1} - 1)$ steps of the SQW and $(2^N - 1)$ steps of the DQW can be implemented.

Each step of the SQW is evolved using a coin operation C_θ followed by the shift operation S as given in Eq. (3). Since S acts on the position state and the mapping of the position to the qubit state is not unique, the composition of gates for the design of S is also not unique. The coin operation C_θ can be carried out by using a single-qubit gate operation on the coin qubit, while the position shift operation S can be subsequently applied with the help of multiqubit gates where the coin qubit acts as the control. For instance, Fig. 5 presents a naive quantum circuit for a single step of the SQW on a five-qubit quantum processor [63]. The general form of this circuit depends on the mapping of the position state to the qubit states (see Table I).

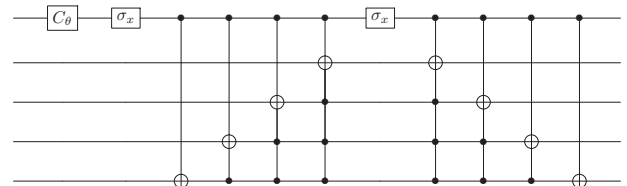


FIG. 5. Generic quantum circuit to implement one step of the SQW on a five-qubit system for the mapping given in Table I. Repetition of this circuit will give us the SQW on the position Hilbert space with 16 sites. The shift operation S is performed using the increment and decrement circuit.

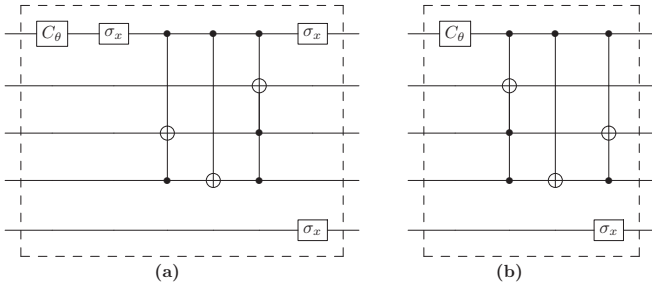


FIG. 6. Generic quantum circuit for two steps of the SQW on a five-qubit system for the mapping given in Table II. It can be used to implement up to seven steps of the SQW by alternating the circuits in (a) and (b). If the initial position state is even, the circuit in (a) is applied first, and if the initial position state is odd, the circuit in (b) is applied first.

We note that the mapping of the position to the qubit state is not unique and the quantum circuit can be simplified using different mapping. Here the odd (even) position state is identified with the configuration of the last qubit being $|1\rangle$ ($|0\rangle$). Repeating the circuit in Fig. 5 will give seven steps of the SQW, but it can be scaled to N qubits using an increment and decrement circuit. However, for this mapping the gate size and gate counting per step of the SQW increase with the number of qubits. At this point, we have claimed that the quantum circuit complexity of the DTQW depends on the position space mapping. Therefore, we will now show that a mapping that takes the architecture of the quantum processor into account reduces the gate size and gate count. Additional reductions can be achieved by fixing the initial state of the walk. Here we present a quantum circuit on a five-qubit system for the SQW and DQW that can be easily realized on present-day quantum processors, e.g., the five-qubit programmable trapped-ion quantum computer [60] or IBM Quantum’s five-qubit quantum computer [64,65].

Figure 6 shows a quantum circuit for two steps of the SQW for the mapping presented in Table II. Similar to the previous case, the state of the last qubit defines the even and odd positions. This allows us to keep the rest of the mapped qubits identical for each pair of even and odd positions. For a generic initial position state $|x\rangle$ of the particle on a five-qubit system, the alternation of the circuits in Figs. 6(a) and 6(b) implements

TABLE I. Mapping of the position state to the multiqubit state for the quantum circuit presented in Fig. 5. This multiqubit configuration identifies the even and odd position states in the system with the help of $|0\rangle$ and $|1\rangle$ as the state of the last qubit, respectively.

$ x = 0\rangle \equiv 0000\rangle$	
$ x = 1\rangle \equiv 0001\rangle$	$ x = -1\rangle \equiv 1111\rangle$
$ x = 2\rangle \equiv 0010\rangle$	$ x = -2\rangle \equiv 1110\rangle$
$ x = 3\rangle \equiv 0011\rangle$	$ x = -3\rangle \equiv 1101\rangle$
$ x = 4\rangle \equiv 0100\rangle$	$ x = -4\rangle \equiv 1100\rangle$
$ x = 5\rangle \equiv 0101\rangle$	$ x = -5\rangle \equiv 1011\rangle$
$ x = 6\rangle \equiv 0110\rangle$	$ x = -6\rangle \equiv 1010\rangle$
$ x = 7\rangle \equiv 0111\rangle$	$ x = -7\rangle \equiv 1001\rangle$

TABLE II. Mapping of the position state to the multiqubit state for quantum circuits presented in Figs. 6, 7, 8, and 9. Here also the multiqubit configuration identifies even- and odd-numbered positions in the system with respect to the $|0\rangle$ and $|1\rangle$ states of the last qubit, respectively.

$ x = 0\rangle \equiv 0000\rangle$	
$ x = 1\rangle \equiv 0001\rangle$	$ x = -1\rangle \equiv 0011\rangle$
$ x = 2\rangle \equiv 0110\rangle$	$ x = -2\rangle \equiv 0010\rangle$
$ x = 3\rangle \equiv 0111\rangle$	$ x = -3\rangle \equiv 0101\rangle$
$ x = 4\rangle \equiv 1100\rangle$	$ x = -4\rangle \equiv 0100\rangle$
$ x = 5\rangle \equiv 1101\rangle$	$ x = -5\rangle \equiv 1111\rangle$
$ x = 6\rangle \equiv 1010\rangle$	$ x = -6\rangle \equiv 1110\rangle$
$ x = 7\rangle \equiv 1011\rangle$	$ x = -7\rangle \equiv 1001\rangle$

the seven steps of the SQW. If the initial position $|x\rangle$ is even (odd), the circuit in Fig. 6(a) [Fig. 6(b)] is applied first. When we compare the result to the quantum circuit in Fig. 5 for a naive mapping, we see a significant decrease in the gate count and gate size for each step. The gate count reduces to almost half for each step. Similarly, Fig. 7 shows the quantum circuit for each step of the DQW for mapping presented in Table II for any arbitrary initial position state $|x\rangle$, and with repeated application of this circuit, one can implement 15 steps of the DQW, in principle.

In a comparison of the two quantum circuits for the SQW, one step of the naive mapping shown in Fig. 5 has two of each Toffoli-3 gate, Toffoli-2 gate, Toffoli gate, and controlled NOT (CNOT) gate along with three single-qubit gates, while each step of the generic circuit shown in Fig. 6 for mapping in Table II has only one Toffoli-2 gate, one Toffoli gate, and one CNOT gate along with a few single-qubit gates. Hence, this shows that for a smart position-state mapping, the gate count drops significantly, and hence, the circuit complexity decreases.

Fixing the initial state of the walker helps to reduce the gate count in the quantum circuit and also reduces the circuit complexity. For example, for an initial state fixed to $|0\rangle \otimes |0000\rangle \equiv |\uparrow\rangle \otimes |x = 0\rangle$, the quantum circuits for the first seven steps of the SQW and DQW are shown in Figs. 8 and 9, respectively. But for the implementation of the SSQW,

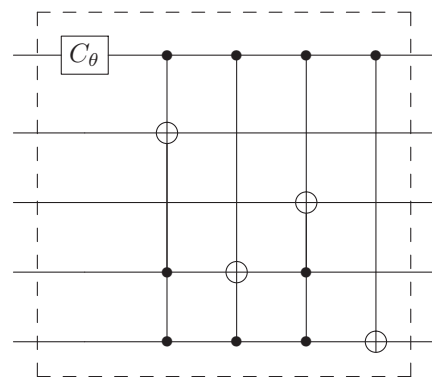


FIG. 7. Generic quantum circuit for a DQW on a five-qubit system for the mapping given in Table II. Concatenation of this circuit will give the probability distribution of the DQW for up to 15 steps.

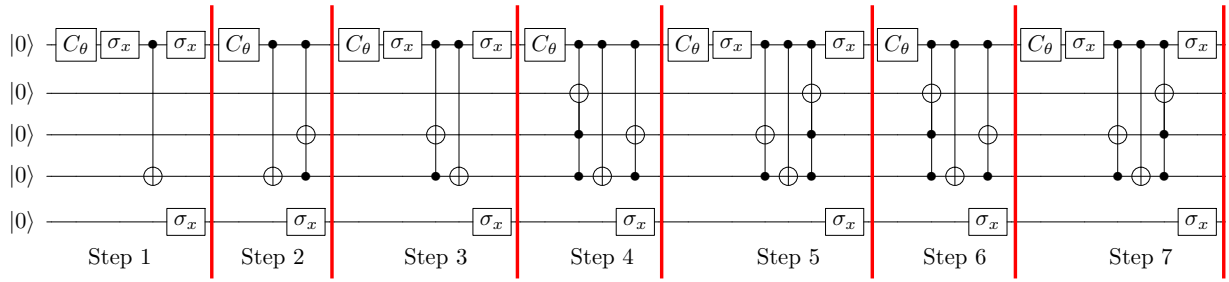


FIG. 8. Quantum circuit for the first seven steps of the SQW on a five-qubit system with the fixed initial state $|\uparrow\rangle \otimes |x=0\rangle \equiv |0\rangle \otimes |0000\rangle$ for the mapping given in Table II. This circuit has a reduced gate count compared to the generic circuit shown in Fig. 6. We note that the sequence of σ_x in the last qubit can be replaced by classically tracking the number of steps.

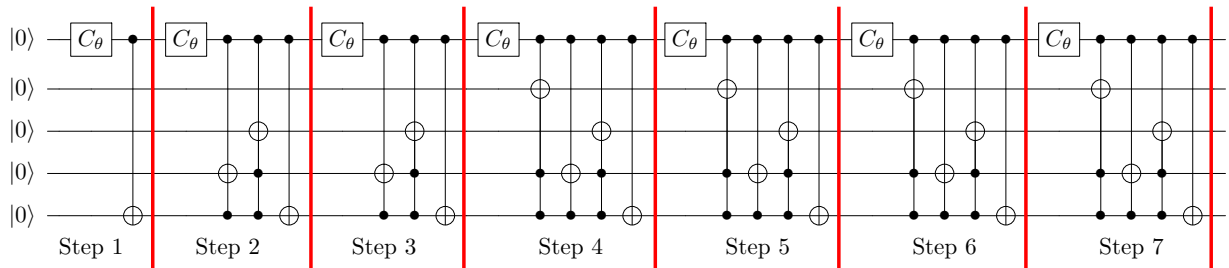


FIG. 9. Quantum circuit for the first seven steps of the DQW on a five-qubit system with the fixed initial state $|\uparrow\rangle \otimes |x=0\rangle \equiv |0\rangle \otimes |0000\rangle$ for the mapping given in Table II. It has a reduced gate count compared to the generic circuit shown in Fig. 7.

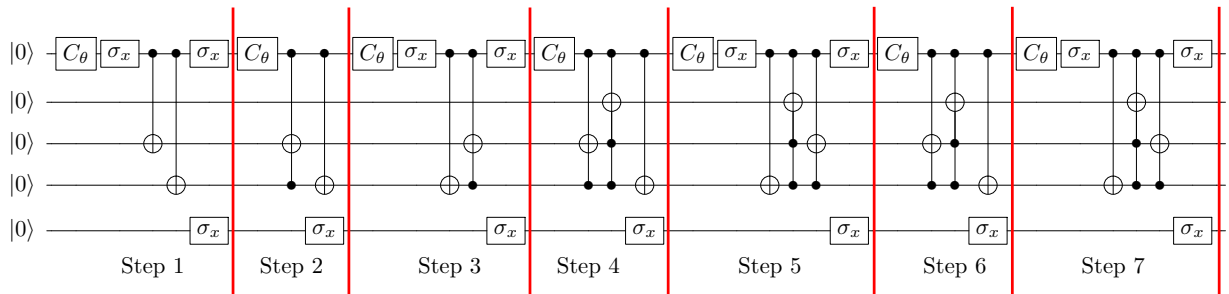


FIG. 10. Quantum circuit for the SQW for the first seven steps on a five-qubit system for the fixed initial state $|\uparrow\rangle \otimes |x=0\rangle \equiv |0\rangle \otimes |0000\rangle$ for the mapping given in Table III. Here also the sequence of σ_x in the last qubit can be completely replaced by classically tracking the step number.

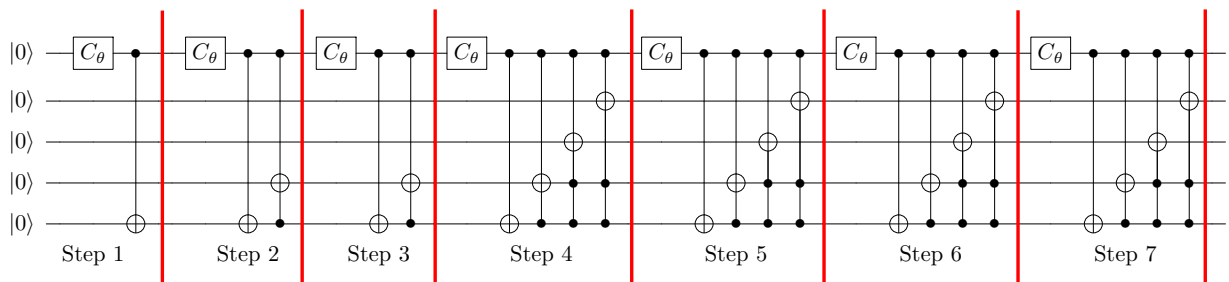


FIG. 11. Quantum circuit for the first seven steps of the DQW on a five-qubit system with the fixed initial state $|\uparrow\rangle \otimes |x=0\rangle \equiv |0\rangle \otimes |0000\rangle$ for the mapping given in Table III.

TABLE III. Mapping of the position state to the multiqubit state for quantum circuits presented in Figs. 10 and 11.

$ x = 0\rangle \equiv 0000\rangle$	
$ x = 1\rangle \equiv 0001\rangle$	$ x = -1\rangle \equiv 0111\rangle$
$ x = 2\rangle \equiv 0010\rangle$	$ x = -2\rangle \equiv 0110\rangle$
$ x = 3\rangle \equiv 0011\rangle$	$ x = -3\rangle \equiv 0101\rangle$
$ x = 4\rangle \equiv 1100\rangle$	$ x = -4\rangle \equiv 0100\rangle$
$ x = 5\rangle \equiv 1101\rangle$	$ x = -5\rangle \equiv 1011\rangle$
$ x = 6\rangle \equiv 1110\rangle$	$ x = -6\rangle \equiv 1010\rangle$
$ x = 7\rangle \equiv 1111\rangle$	$ x = -7\rangle \equiv 1001\rangle$

two different shift operators are needed. The same results can be reconstructed from the equivalence relation between the SSQW and SQW, which will need two steps of the SQW to reproduce the results of the SSQW. Therefore, using the SQW and reconstructing the results of the corresponding SSQW from it are more efficient than the direct implementation of the SSQW.

We have also considered a different configuration of the position space mapping onto multiqubit states. As in Table II the last qubit states, $|0\rangle$ and $|1\rangle$, are set to identify the even and odd position of the position state here too. The mapping given in Table III and Figs. 10 and 11 shows the quantum circuits for the SQW and DQW for the mapping choices, respectively, which implements seven steps for the initial state $|0\rangle \otimes |x = 0\rangle$. At alternate sites of the SQW we have zero probability, and our mapping allows the value of the last qubit to identify odd or even positions. Alternatively, the step number can be classically tracked in the quantum circuits shown in Figs. 6, 8, and 10 to reduce the number of σ_x operations on the last qubit to zero or one.

Among the quantum circuits presented, the one given in Fig. 8 is optimal for implementing the SQW. Table IV gives a comparison of the number of gates in the optimized circuits in Fig. 8, 9, 10, and 11.

IV. DISCUSSION

By digitally encoding the walker’s position space onto the qubit state in various ways, we have shown different equivalent quantum walk circuits. The examples illustrate how the encoding methods and initial-state-dependent circuits can

TABLE IV. Gate count for mapping in Tables II and III and for corresponding SQW and DQW circuits with the fixed initial state $|0\rangle \otimes |0000\rangle$ and after seven steps on a five-qubit quantum processor.

	SQW	DQW
Table II	22 single-qubit	7 single-qubit
	7 two-qubit	7 two-qubit
	6 three-qubit	6 three-qubit
	4 four-qubit	10 four-qubit
Table III	22 single-qubit	7 single-qubit
	8 two-qubit	6 two-qubit
	6 three-qubit	6 three-qubit
	4 four-qubit	8 four-qubit

reduce the required gate depth (gate count) for implementing quantum walks.

The circuits can be scaled to implement more steps on a larger system using higher-order Toffoli gates. The implementation of n steps of a SQW will need at least $\lceil \log_2(n + 1) + 2 \rceil$ qubits. Similarly, to implement n steps of a DQW, at least $\lceil \log_2(n + 1) + 1 \rceil$ qubits are required.

Recently, two different ways of expanding the increasing and decreasing parts of the generic quantum circuit shown in Fig. 5 were explored in detail [66]. In one of the ways, the circuit complexity is reduced by using the generalized controlled inversions method and in the other, the rotation operations around the basis states was used. If the circuits are implemented on a device with a large number of qubits, then generalized controlled inversions would be a good option as they have less circuit depth due to the use of ancilla qubits or else the approach with rotation around basis state would be better. In our work the focus has been on reducing the circuit complexity by a careful choice of mapping of the qubit state to the position space and optimizing the circuit after choosing the initial state. Combining both these approaches may results in a further reduction of the circuit complexity, and that needs to be carefully explored in future works.

DTQWs in two-dimensional position space [67,68] can also be implemented by scaling the scheme presented in this work with an appropriate mapping of qubit states with the nearest-neighbor position space in both dimensions. This can be achieved on a device with access to a larger number of qubits by assigning an equal number of qubits to both dimensions in the two-dimensional position space and then by optimally mapping the qubit state to the position state. All the circuits presented can be extended to implement two or more particle DTQWs by introducing two or more coin qubits into the system. In such cases, the control over the target or position qubit increases with the number of coin qubits. Another way of scaling the scheme for the SQW on an N -qubit system is to fix one qubit for the coin as usual and another one to represent the \pm sign for the positive and negative directions of the initial state $|x\rangle$, and the states of the rest of the $(N - 2)$ qubits can be mapped to the position state. Now using the quantum adder circuit [69], the scheme can be extended to N qubits, and a generalized quantum circuit for the quantum walk can be worked out.

One can also use ancilla qubits to reduce the circuit complexity. In the Appendix, we show a hybrid circuit with the help ancilla qubits for the DQW. The DQW can be implemented with the help of a CNOT gate, and interference in the walk can be included with the help of a controlled-SWAP gate and an ancilla qubit just before the measurement. Figures 14 and 15 show the hybrid circuit for four steps and three steps of the DQW. Details are given in the Appendix.

TABLE V. Mapping of the position state onto multiqubit states for the DQW circuit presented in Fig. 12.

$ x = 0\rangle \equiv 0000\rangle$	
$ x = 1\rangle \equiv 1000\rangle$	$ x = 4\rangle \equiv 1111\rangle$
$ x = 2\rangle \equiv 1100\rangle$	$ x = 5\rangle \equiv 0111\rangle$
$ x = 3\rangle \equiv 1110\rangle$	$ x = 6\rangle \equiv 1011\rangle$

TABLE VI. Position state mapping used to construct the quantum circuit presented in Fig. 13. This mapping requires ancilla qubits to induce interference by merging equivalent multiqubit states.

$ x = 0\rangle \equiv 0000\rangle$
$ x = 1\rangle \equiv \{ 1000\rangle, 0100\rangle, 0010\rangle, 0001\rangle\}$
$ x = 2\rangle \equiv \{ 1100\rangle, 1010\rangle, 1001\rangle,$ $ 0110\rangle, 0101\rangle, 0011\rangle\}$
$ x = 3\rangle \equiv \{ 1110\rangle, 1101\rangle, 1011\rangle, 0111\rangle\}$
$ x = 4\rangle \equiv 1111\rangle$

Therefore, with an appropriate choice of the quantum coin operation and the equivalence of variants of DTQW, any quantum algorithm based on the DTQW can be experimentally realized on a quantum computer. Dirac cellular automata can be recovered using the SSQW, which reproduces the dynamics of the Dirac equation in the continuum limit [40]. One such example of simulating Dirac cellular automata on an ion-trap processor using one of the various configurations of the circuits presented was demonstrated recently [70]. With the appropriate use of a position-dependent coin operation and additional higher-order Toffoli gates in our circuits, other DTQW-based algorithms, such as spatial search, can also be implemented.

ACKNOWLEDGMENTS

C.H.A. acknowledges financial support from CONACYT Doctoral Grant No. 455378. N.M.L. acknowledges financial support from NSF Grant No. PHY-1430094 to the PFC@JQI. C.M.C. acknowledges the support from the Department of Science and Technology, Government of India, under Ramanujan Fellowship Grant No. SB/S2/RJN-192/2014 and U.S. Army ITC-PAC Grant No. FA520919PA139.

APPENDIX

1. DQW circuit with naive mapping

A naive mapping can result in an inefficient quantum circuit. One example of this is given in Table V and Fig. 12.

The simplest quantum circuit for the mapping given above with fixed initial state $|0\rangle \otimes |0000\rangle$ is shown in Fig. 12. This circuit implements five steps of the DQW. In the same system one can implement up to 15 steps since the available position

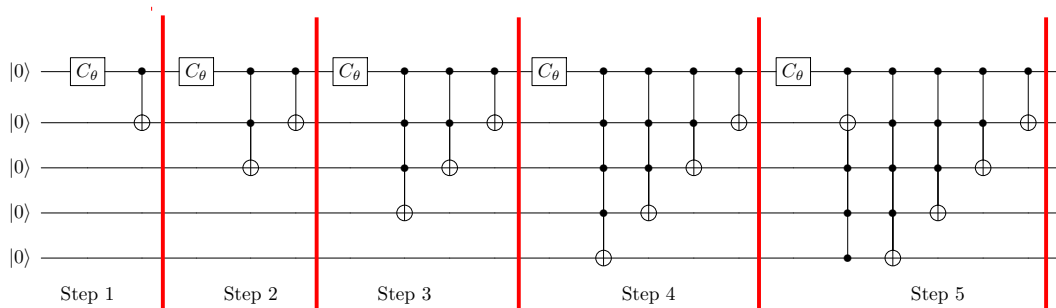


FIG. 12. Quantum circuit for the DQW for the first five steps with the fixed initial state $|\Psi_{in}\rangle = |\uparrow\rangle \otimes |x = 0\rangle \equiv |0\rangle \otimes |0000\rangle$ for the naive mapping shown in Table V. This circuit has a simple structure, but it consists of many additional higher-order Toffoli gates compared to the circuits shown in Sec. III and the Appendix.

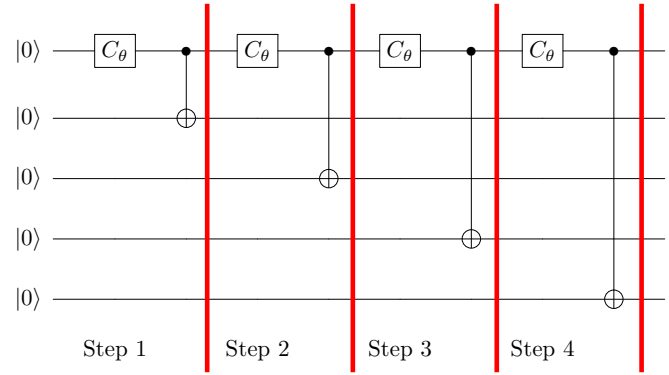


FIG. 13. Quantum circuit for the DQW for the first four steps without interference. Each step of this quantum circuit is given by a CNOT gate because of the mapping chosen (see Table VI). To include interference in the circuit, ancilla operations are needed before the measurement (see Fig. 14).

states are $2^4 = 16$. This circuit looks straightforward to construct and scale, but an actual implementation would require higher-order Toffoli gates even for a small number of steps and a fixed initial position, making it inefficient for near-term quantum processors.

2. Simplified quantum circuit with an ancilla

There has been a significant increase in the number of qubits available on platforms like trapped-ion and superconducting qubits [71–74]. However, limited coherence time is still a hindrance to increasing the number of gates that can be implemented. To make explicit use of the all available qubits, one has to develop low-depth quantum circuits. Here we will present quantum circuits with a reduced number of gates to implement DQWs at the cost of requiring additional ancilla qubits. But the given circuit is still inefficient as it will include only outputs with ancilla qubit state $|0\rangle$. In a system with access to more qubits, one can implement more steps of the DQW at the same circuit depth, but the efficiency decreases as the number of output states that can be included decreases when all the ancilla qubit states are $|0\rangle$.

For a five-qubit system, we again use the first qubit to represent the coin and the other four qubits to represent position space. The mapping is given in Table VI. This is a classical

TABLE VII. Output after each step of the DQW and output of the quantum circuit shown in Fig. 13 without the interference step provided by the ancilla circuit. Here c_1, c_2, \dots represent the contributions of the $\cos(\theta)$ term from the coin operation in the first and second time evolutions and so on, and similarly, s_1, s_2, \dots represent the contributions of the $\sin(\theta)$ term from the coin operation in the first and second time evolutions and so on, respectively, in the circuit.

Step	Directed quantum walk output	Circuit output without ancilla
0	$ 0\rangle \otimes x=0\rangle$	$ 0\rangle \otimes 0000\rangle$
1	$c_1 0\rangle \otimes x=0\rangle + s_1 1\rangle \otimes x=1\rangle$	$c_1 0\rangle \otimes 0000\rangle + s_1 1\rangle \otimes 1000\rangle$
2	$c_2c_1 0\rangle \otimes x=0\rangle + s_2c_1 1\rangle \otimes x=1\rangle + s_2s_1 0\rangle \otimes x=1\rangle - c_2s_1 1\rangle \otimes x=2\rangle$	$c_2c_1 0\rangle \otimes 0000\rangle + s_2c_1 1\rangle \otimes 0100\rangle + s_2s_1 0\rangle \otimes 1000\rangle - c_2s_1 1\rangle \otimes 1100\rangle$
3	$c_3c_2c_1 0\rangle \otimes x=0\rangle + s_3c_2c_1 1\rangle \otimes x=1\rangle + s_3s_2c_1 0\rangle \otimes x=1\rangle - c_3s_2c_1 1\rangle \otimes x=2\rangle + c_3s_2s_1 0\rangle \otimes x=1\rangle + s_3s_2s_1 1\rangle \otimes x=2\rangle - s_3c_2s_1 0\rangle \otimes x=2\rangle + c_3c_2s_1 1\rangle \otimes x=3\rangle$	$c_3c_2c_1 0\rangle \otimes 0000\rangle + s_3c_2c_1 1\rangle \otimes 0010\rangle + s_3s_2c_1 0\rangle \otimes 0100\rangle - c_3s_2c_1 1\rangle \otimes 0110\rangle + c_3s_2s_1 0\rangle \otimes 1000\rangle + s_3s_2s_1 1\rangle \otimes 1010\rangle - s_3c_2s_1 0\rangle \otimes 1100\rangle + c_3c_2s_1 1\rangle \otimes 1110\rangle$
4	$c_4c_3c_2c_1 0\rangle \otimes x=0\rangle + s_4c_3c_2c_1 1\rangle \otimes x=1\rangle + s_4s_3c_2c_1 0\rangle \otimes x=1\rangle - c_4s_3c_2c_1 1\rangle \otimes x=2\rangle + c_4s_3s_2c_1 0\rangle \otimes x=1\rangle + s_4s_3s_2c_1 1\rangle \otimes x=2\rangle - s_4c_3s_2c_1 0\rangle \otimes x=2\rangle + c_4c_3s_2c_1 1\rangle \otimes x=3\rangle + c_4c_3s_2s_1 0\rangle \otimes x=1\rangle + s_4c_3s_2s_1 1\rangle \otimes x=2\rangle + s_4s_3s_2s_1 0\rangle \otimes x=2\rangle - c_4s_3s_2s_1 1\rangle \otimes x=3\rangle - c_4s_3c_2s_1 0\rangle \otimes x=2\rangle - s_4s_3c_2s_1 1\rangle \otimes x=3\rangle + s_4c_3c_2s_1 0\rangle \otimes x=3\rangle - c_4c_3c_2s_1 1\rangle \otimes x=4\rangle$	$c_4c_3c_2c_1 0\rangle \otimes 0000\rangle + s_4c_3c_2c_1 1\rangle \otimes 0001\rangle + s_4s_3c_2c_1 0\rangle \otimes 0010\rangle - c_4s_3c_2c_1 1\rangle \otimes 0011\rangle + c_4s_3s_2c_1 0\rangle \otimes 0100\rangle + s_4s_3s_2c_1 1\rangle \otimes 0101\rangle - s_4c_3s_2c_1 0\rangle \otimes 0110\rangle + c_4c_3s_2c_1 1\rangle \otimes 0111\rangle + c_4c_3s_2s_1 0\rangle \otimes 1000\rangle + s_4c_3s_2s_1 1\rangle \otimes 1001\rangle + s_4s_3s_2s_1 0\rangle \otimes 1010\rangle - c_4s_3s_2s_1 1\rangle \otimes 1011\rangle - c_4s_3c_2s_1 0\rangle \otimes 1100\rangle - s_4s_3c_2s_1 1\rangle \otimes 1101\rangle + s_4c_3c_2s_1 0\rangle \otimes 1110\rangle - c_4c_3c_2s_1 1\rangle \otimes 1111\rangle$

circuit as it does not include the superposition or interference in the system directly. The output of the DQW and that of the quantum circuit in Fig. 13 are compared in Table VII for each step. To keep track of the contribution from each time evolution, we have introduced subscripts to indicate different time steps. To turn this circuit into a DQW implementation,

CNOT and Fredkin (controlled-SWAP) gates and a Hadamard gate involving additional ancilla qubits are applied before the measurement, as shown in Fig. 14. After the measurement, only selective outputs with ancilla qubit state $|0\rangle$ are included.

After the first three steps, a single ancilla qubit introduces the equivalence of the states with two qubits in state $|1\rangle$ to

TABLE VIII. Output after the three steps of a DQW using the quantum circuit shown in Fig. 13 and the output of the quantum circuit with an ancilla, as shown in Fig. 14 after the interference step. Here c_1, c_2, \dots represent the contributions of the $\cos(\theta)$ term from the coin operation in the first and second time evolutions and so on, and similarly, s_1, s_2, \dots represent the contributions of the $\sin(\theta)$ term from the coin operation in the first and second time evolutions and so on, respectively, in the circuit.

Step	Circuit output without ancilla	Circuit output with ancilla
3	$(c_3c_2c_1 0\rangle \otimes 0000\rangle + s_3c_2c_1 1\rangle \otimes 0010\rangle + s_3s_2c_1 0\rangle \otimes 0100\rangle - c_3s_2c_1 1\rangle \otimes 0110\rangle + c_3s_2s_1 0\rangle \otimes 1000\rangle + s_3s_2s_1 1\rangle \otimes 1010\rangle - s_3c_2s_1 0\rangle \otimes 1100\rangle + c_3c_2s_1 1\rangle \otimes 1110\rangle) \otimes 0\rangle$	$(c_3c_2c_1 0\rangle \otimes 0000\rangle \otimes 0\rangle + s_3c_2c_1 1\rangle \otimes 0010\rangle \otimes 0\rangle + s_3s_2c_1 0\rangle \otimes 0100\rangle \otimes 0\rangle + c_3s_2s_1 1\rangle \otimes 0110\rangle \otimes 1\rangle + s_3s_2s_1 0\rangle \otimes 1000\rangle \otimes 1\rangle - c_3s_2c_1 1\rangle \otimes 1010\rangle \otimes 0\rangle - s_3c_2s_1 0\rangle \otimes 1100\rangle \otimes 1\rangle + c_3c_2s_1 1\rangle \otimes 1110\rangle \otimes 1\rangle)$

TABLE IX. Output after the four steps of a DQW using the quantum circuit shown in Fig. 13 and the output of the quantum circuit with an ancilla, as shown in Fig. 15 after the interference step. Here c_1, c_2, \dots represent the contributions of the $\cos(\theta)$ term from the coin operation in the first and second time evolutions and so on, and similarly, s_1, s_2, \dots represent the contributions of the $\sin(\theta)$ term from the coin operation in the first and second time evolutions and so on, respectively, in the circuit.

Step	Circuit output without ancilla	Circuit Output with ancilla
4	$(c_4c_3c_2c_1 0\rangle \otimes 0000\rangle +$ $s_4c_3c_2c_1 1\rangle \otimes 0001\rangle +$ $s_4s_3c_2c_1 0\rangle \otimes 0010\rangle -$ $c_4s_3c_2c_1 1\rangle \otimes 0011\rangle +$ $c_4s_3s_2c_1 0\rangle \otimes 0100\rangle +$ $s_4s_3s_2c_1 1\rangle \otimes 0101\rangle -$ $s_4c_3s_2c_1 0\rangle \otimes 0110\rangle +$ $c_4c_3s_2c_1 1\rangle \otimes 0111\rangle +$ $c_4c_3s_2s_1 0\rangle \otimes 1000\rangle +$ $s_4c_3s_2s_1 1\rangle \otimes 1001\rangle +$ $s_4s_3s_2s_1 0\rangle \otimes 1010\rangle -$ $c_4s_3s_2s_1 1\rangle \otimes 1011\rangle -$ $c_4s_3c_2s_1 0\rangle \otimes 1100\rangle -$ $s_4s_3c_2s_1 1\rangle \otimes 1101\rangle +$ $s_4c_3c_2s_1 0\rangle \otimes 1110\rangle -$ $c_4c_3c_2s_1 1\rangle \otimes 1111\rangle) \otimes 000\rangle$	$c_4c_3c_2c_1 0\rangle \otimes 0000\rangle \otimes 000\rangle +$ $s_4c_3c_2c_1 1\rangle \otimes 0001\rangle \otimes 000\rangle +$ $s_4s_3c_2c_1 0\rangle \otimes 0100\rangle \otimes 001\rangle +$ $c_4s_3s_2c_1 0\rangle \otimes 0100\rangle \otimes 000\rangle +$ $c_4c_3s_2s_1 0\rangle \otimes 0100\rangle \otimes 100\rangle +$ $s_4c_3s_2s_1 1\rangle \otimes 0101\rangle \otimes 100\rangle -$ $s_4s_3c_2c_1 1\rangle \otimes 0101\rangle \otimes 001\rangle +$ $s_4s_3s_2c_1 1\rangle \otimes 0101\rangle \otimes 000\rangle +$ $s_4s_3s_2s_1 0\rangle \otimes 0110\rangle \otimes 101\rangle -$ $s_4c_3s_2c_1 0\rangle \otimes 0110\rangle \otimes 001\rangle -$ $c_4s_3c_2s_1 0\rangle \otimes 0110\rangle \otimes 010\rangle +$ $c_4c_3s_2c_1 1\rangle \otimes 0111\rangle \otimes 001\rangle -$ $c_4s_3s_2s_1 1\rangle \otimes 0111\rangle \otimes 101\rangle -$ $s_4s_3c_2s_1 1\rangle \otimes 0111\rangle \otimes 110\rangle +$ $s_4c_3c_2s_1 0\rangle \otimes 1110\rangle \otimes 111\rangle -$ $c_4c_3c_2s_1 1\rangle \otimes 1111\rangle \otimes 111\rangle$

position space at $|x=2\rangle$, as shown in Fig. 14. After the operation on the ancilla qubit, the DQW distribution after three steps is recovered. Table VIII shows the equivalence of the output of the third step of the DQW to the circuit output after the first three steps with an ancilla qubit operation before the Hadamard operation is performed on an ancilla qubit.

Similarly, to include interference after four steps, we need three ancilla qubits, as shown in Fig. 15, and the output equivalence is shown in Table IX before the Hadamard gate is performed on the ancilla qubit. The Hadamard operation helps in unentangling the ancilla qubit with the real qubits in the circuit.

The number of ancilla qubits as well as Fredkin (CSWAP) gates for the circuit in Fig. 13 increases as $n^{-1}C_2$, where n is the step number after which the measurement is done. The ancilla operation is needed only before the measurement.

From Fig. 15, it can be seen that for the first four steps of the DQW, the number of CNOT gates required is seven, along with three Fredkin gates. Each Fredkin gate can be

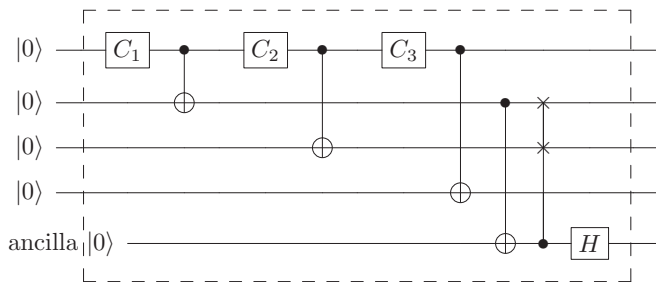


FIG. 14. Quantum circuit for the DQW with the ancilla operation to include interference after the first three steps. The ancilla qubit is left unobserved in the circuit. Here $C_1 = C_2 = C_3 = C_\theta$.

decomposed into five two-qubit gates [75]. Therefore, the total number of two-qubit gates required for the first four steps of the DQW using ancilla qubits is 22. Compared to this, if we look at the DQW circuit without ancilla qubits, for the first four steps the number of CNOT gates required is four, the number of Toffoli gate is three, and the number of controlled-Toffoli (CCNOT) gates is two, as can be seen in Figs. 9 and 11. Each Toffoli gate can be decomposed into six CNOT gates, and each CCNOT gate can be further decomposed into a two-qubit gate and Toffoli gates [76]. The number of two-qubit gates required for the first four steps of the DQW without the use of ancilla qubits will be far greater than 22. Therefore, a processor with access to a large number of qubits with the possibility to leave the ancilla qubit unobserved [77,78] could be effective in reducing the gate counts to implement the DTQW.

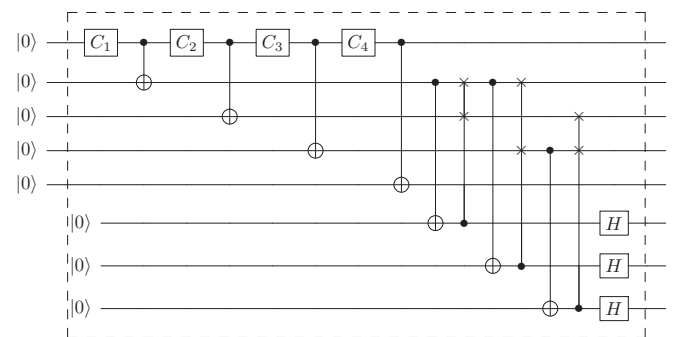


FIG. 15. Quantum circuit for the DQW with the ancilla operation to include interference after the first four steps. The ancilla qubits are left unobserved in the circuit. With a larger number of steps, the number of ancilla qubits also increases. Here $C_1 = C_2 = C_3 = C_4 = C_\theta$.

- [1] J. Preskill, Quantum computing in the NISQ era and beyond, *Quantum* **2**, 79 (2018).
- [2] Y. Alexeev *et al.*, Quantum computer systems for scientific discovery, *PRX Quantum* **2**, 017001 (2021).
- [3] J. Kempe, Quantum random walks: An introductory overview, *Contemp. Phys.* **44**, 307 (2003).
- [4] S. E. Venegas-Andraca, Quantum walks: A comprehensive review, *Quant. Inf. Process.* **11**, 1015 (2012).
- [5] A. M. Childs, R. Cleve, E. Deotto, E. Farhi, S. Gutmann, and D. A. Spielman, Exponential algorithmic speedup by a quantum walk, in *Proceedings of the Thirty-Fifth Annual ACM Symposium on Theory of Computing* (ACM, New York, 2003), pp. 59–68.
- [6] A. Ambainis, Quantum walks and their algorithmic applications, *Int. J. Quantum Inf.* **1**, 507 (2003).
- [7] N. Shenvi, J. Kempe, and K. B. Whaley, Quantum random-walk search algorithm, *Phys. Rev. A* **67**, 052307 (2003).
- [8] A. Ambainis, Quantum walk algorithm for element distinctness, *SIAM J. Comput.* **37**, 210 (2007).
- [9] F. Magniez, M. Santha, and M. Szegedy, Quantum algorithms for the triangle problem, *SIAM J. Comput.* **37**, 413 (2007).
- [10] B. L. Douglas and J. B. Wang, A classical approach to the graph isomorphism problem using quantum walks, *J. Phys. A* **41**, (2008).
- [11] J. K. Gamble, M. Friesen, D. Zhou, R. Joynt, and S. Coppersmith, Two-particle quantum walks applied to the graph isomorphism problem, *Phys. Rev. A* **81**, 052313 (2010).
- [12] S. D. Berry and J. B. Wang, Two-particle quantum walks: Entanglement and graph isomorphism testing, *Phys. Rev. A* **83**, 042317 (2011).
- [13] G. D. Paparo and M. Martin-Delgado, Google in a quantum network, *Sci. Rep.* **2**, 444 (2012).
- [14] G. D. Paparo, M. Müller, F. Comellas, and M. A. Martin-Delgado, Quantum Google in a complex network, *Sci. Rep.* **3**, 2773 (2013).
- [15] T. Loke, J. Tang, J. Rodriguez, M. Small, and J. B. Wang, Comparing classical and quantum pageranks, *Quantum Inf. Process.* **16**, 25 (2017).
- [16] P. Chawla, R. Mangal, and C. M. Chandrashekar, Discrete-time quantum walk algorithm for ranking nodes on a network, *Quantum Inf. Proc.* **19**, 158 (2020).
- [17] P. Arrighi, S. Facchini, and M. Forets, Quantum walking in curved spacetime, *Quantum Inf. Process.* **15**, 3467 (2016).
- [18] G. Di Molfetta, M. Brachet, and F. Debbasch, Quantum walks in artificial electric and gravitational fields, *Phys. A (Amsterdam, Neth.)* **397**, 157 (2014).
- [19] G. Di Molfetta, M. Brachet, and F. Debbasch, Quantum walks as massless Dirac fermions in curved space-time, *Phys. Rev. A* **88**, 042301 (2013).
- [20] C. M. Chandrashekar, Two-component Dirac-like Hamiltonian for generating quantum walk on one-, two- and three-dimensional lattices, *Sci. Rep.* **3**, 2829 (2013).
- [21] C. M. Chandrashekar, S. Banerjee, and R. Srikanth, Relationship between quantum walks and relativistic quantum mechanics, *Phys. Rev. A* **81**, 062340 (2010).
- [22] F. W. Strauch, Relativistic quantum walks, *Phys. Rev. A* **73**, 054302 (2006).
- [23] G. Di Molfetta and A. Pérez, Quantum walks as simulators of neutrino oscillations in a vacuum and matter, *New J. Phys.* **18**, 103038 (2016).
- [24] A. Mallick, S. Mandal, A. Karan, and C. M. Chandrashekar, Simulating Dirac Hamiltonian in curved space-time by split-step quantum walk, *J. Phys. Commun.* **3**, 015012 (2019).
- [25] C. M. Chandrashekar and T. Busch, Localized quantum walks as secured quantum memory, *Europhys. Lett.* **110**, 10005 (2015).
- [26] A. Mallick, S. Mandal, and C. M. Chandrashekar, Neutrino oscillations in discrete-time quantum walk framework, *Eur. Phys. J. C* **77**, 85 (2017).
- [27] D. Aharonov, A. Ambainis, J. Kempe, and U. Vazirani, Quantum walks on graphs, in *Proceedings of the Thirty-Third Annual ACM Symposium on Theory of Computing (STOC '01)* (ACM, New York, 2001), pp. 50–59.
- [28] B. Tregenna, W. Flanagan, R. Maile, and V. Kendon, Controlling discrete quantum walks: Coins and initial states, *New J. Phys.* **5**, 83 (2003).
- [29] E. Farhi and S. Gutmann, Quantum computation and decision trees, *Phys. Rev. A* **58**, 915 (1998).
- [30] H. Gerhardt and J. Watrous, Continuous-time quantum walks on the symmetric group, in *Approximation, Randomization, and Combinatorial Optimization: Algorithms and Techniques, Random 2003, Approx 2003*, edited by S. Arora, K. Jansen, J. D. P. Rolim, and A. Sahai, Lecture Notes in Computer Science, Vol. 2764 (Springer, Berlin, Heidelberg, 2003), pp. 290–301.
- [31] G. V. Ryazanov, The Feynman path integral for the Dirac equation, *J. Exp. Theor. Phys.* **6**, 1107 (1958).
- [32] R. P. Feynman, Quantum mechanical computers, *Found. Phys.* **16**, 507 (1986).
- [33] K. R. Parthasarathy, The passage from random walk to diffusion in quantum probability, *J. Appl. Probability* **25**, 151 (1988).
- [34] Y. Aharonov, L. Davidovich, and N. Zagury, Quantum random walks, *Phys. Rev. A* **48**, 1687 (1993).
- [35] S. Hoyer and D. A. Meyer, Faster transport with a directed quantum walk, *Phys. Rev. A* **79**, 024307 (2009).
- [36] A. Montanaro, Quantum walks on directed graphs, *Quantum Inf. Comput.* **7**, 93 (2007).
- [37] C. M. Chandrashekar and T. Busch, Quantum percolation and transition point of a directed discrete-time quantum walk, *Sci. Rep.* **4**, 6583 (2014).
- [38] T. Kitagawa, M. A. Broome, A. Fedrizzi, M. S. Rudner, E. Berg, I. Kassal, A. Aspuru-Guzik, E. Demler, and A. G. White, Observation of topologically protected bound states in photonic quantum walks, *Nat. Commun.* **3**, 882 (2012).
- [39] J. K. Asbóth, Symmetries, topological phases, and bound states in the one-dimensional quantum walk, *Phys. Rev. B* **86**, 195414 (2012).
- [40] A. Mallick and C. M. Chandrashekar, Dirac cellular automaton from split-step quantum walk, *Sci. Rep.* **6**, 25779 (2016).
- [41] M. Szegedy, Quantum speed-up of Markov chain based algorithms, in *Proceedings of the 45th Annual IEEE Symposium on Foundations of Computer Science, 2004* (IEEE, Piscataway, NJ, 2004), pp. 32–41.
- [42] D. A. Meyer, From quantum cellular automata to quantum lattice gases, *J. Stat. Phys.* **85**, 551 (1996).
- [43] A. Pérez, Asymptotic properties of the Dirac quantum cellular automaton, *Phys. Rev. A* **93**, 012328 (2016).
- [44] C. M. Chandrashekar, Disorder induced localization and enhancement of entanglement in one- and two-dimensional quantum walks, [arXiv:1212.5984](https://arxiv.org/abs/1212.5984).

- [45] A. Joye, Dynamical localization for d -dimensional random quantum walks, *Quantum Inf. Process.* **11**, 1251 (2012).
- [46] H. Obuse and N. Kawakami, Topological phases and delocalization of quantum walks in random environments, *Phys. Rev. B* **84**, 195139 (2011).
- [47] T. Kitagawa, M. S. Rudner, E. Berg, and E. Demler, Exploring topological phases with quantum walks, *Phys. Rev. A* **82**, 033429 (2010).
- [48] H. B. Perets, Y. Lahini, F. Pozzi, M. Sorel, R. Morandotti, and Y. Silberberg, Realization of Quantum Walks with Negligible Decoherence in Waveguide Lattices, *Phys. Rev. Lett.* **100**, 170506 (2008).
- [49] M. Karski, L. Forster, J.-M. Choi, A. Steffen, W. Alt, D. Meschede, and A. Widera, Quantum walk in position space with single optically trapped atoms, *Science* **325**, 174 (2009).
- [50] J. Du, H. Li, X. Xu, M. Shi, J. Wu, X. Zhou, and R. Han, Experimental implementation of the quantum random-walk algorithm, *Phys. Rev. A* **67**, 042316 (2003).
- [51] C. A. Ryan, M. Laforest, J.-C. Boileau, and R. Laflamme, Experimental implementation of a discrete-time quantum random walk on an NMR quantum-information processor, *Phys. Rev. A* **72**, 062317 (2005).
- [52] A. Schreiber, K. N. Cassemiro, V. Potocek, A. Gabris, P. J. Mosley, E. Andersson, I. Jex, and C. Silberhorn, Photons Walking the Line: A Quantum Walk with Adjustable Coin Operations, *Phys. Rev. Lett.* **104**, 050502 (2010).
- [53] A. Peruzzo, M. Lobino, J. C. Matthews, N. Matsuda, A. Politi, K. Poulios, X.-Q. Zhou, Y. Lahini, N. Ismail, K. Worhoff, Y. Bromberg, Y. Silberberg, M. G. Thompson, and J. L. O'Brien, Quantum walks of correlated photons, *Science* **329**, 1500 (2010).
- [54] M. A. Broome, A. Fedrizzi, B. P. Lanyon, I. Kassal, A. Aspuru-Guzik, and A. G. White, Discrete Single-Photon Quantum Walks with Tunable Decoherence, *Phys. Rev. Lett.* **104**, 153602 (2010).
- [55] X. Qiang, T. Loke, A. Montanaro, K. Aungskunsiri, X. Zhou, J. L. O'Brien, J. B. Wang, and J. C. F. Matthews, Efficient quantum walk on a quantum processor, *Nat. Commun.* **7**, 11511 (2016).
- [56] X. Qiang, X. Zhou, J. Wang, C. M. Wilkes, T. Loke, S. O'Gara, L. Kling, G. D. Marshall, R. Santagati, T. C. Ralph, J. B. Wang, J. L. O'Brien, M. G. Thompson, and J. C. F. Matthews, Large-scale silicon quantum photonics implementing arbitrary two-qubit processing, *Nat. Photonics* **12**, 534 (2018).
- [57] H. Schmitz, R. Matjeschk, C. Schneider, J. Glueckert, M. Enderlein, T. Huber, and T. Schaetz, Quantum Walk of a Trapped Ion in Phase Space, *Phys. Rev. Lett.* **103**, 090504 (2009).
- [58] F. Zahringer, G. Kirchmair, R. Gerritsma, E. Solano, R. Blatt, and C. F. Roos, Realization of a Quantum Walk with One and Two Trapped Ions, *Phys. Rev. Lett.* **104**, 100503 (2010).
- [59] J.-Q. Zhou, L. Cai, Q.-P. Su, and C.-P. Yang, Protocol of a quantum walk in circuit QED, *Phys. Rev. A* **100**, 012343 (2019).
- [60] S. Debnath, N. M. Linke, C. Figgatt, K. A. Landsman, K. Wright, and C. Monroe, Demonstration of a small programmable quantum computer with atomic qubits, *Nature (London)* **536**, 63 (2016).
- [61] C. M. Chandrashekar, R. Srikanth, and R. Laflamme, Optimizing the discrete-time quantum walk using a SU(2) coin, *Phys. Rev. A* **77**, 032326 (2008).
- [62] N. P. Kumar, R. Balu, R. Laflamme, and C. M. Chandrashekar, Bounds on the dynamics of periodic quantum walks and emergence of the gapless and gapped Dirac equation, *Phys. Rev. A* **97**, 012116 (2018).
- [63] B. L. Douglas and J. B. Wang, Efficient quantum circuit implementation of quantum walks, *Phys. Rev. A* **79**, 052335 (2009).
- [64] F. Acasiete, F. P. Agostini, J. K. Moqadam and R. Portugal, Implementation of quantum walks on IBM quantum computers, *Quantum Inf. Process.* **19**, 426 (2020).
- [65] The IBM Quantum experience, <http://www.research.ibm.com/quantum>.
- [66] K. Georgopoulos, C. Emary, and P. Zuliani, Comparison of quantum-walk implementations on noisy intermediate-scale quantum computers, *Phys. Rev. A* **103**, 022408 (2021).
- [67] C. Di Franco, M. McGettrick, and Th. Busch, Mimicking the Probability Distribution of a Two-Dimensional Grover Walk with a Single-Qubit Coin, *Phys. Rev. Lett.* **106**, 080502 (2011).
- [68] C. M. Chandrashekar and Th. Busch, Decoherence on a two-dimensional quantum walk using four- and two-state particle, *J. Phys. A* **46**, 105306 (2013).
- [69] K.-W. Cheng and C.-C. Tseng, *Electron. Lett.* **38**, 1343 (2002).
- [70] C. H. Alderete, S. Singh, N. H. Nguyen, D. Zhu, R. Balu, C. Monroe, C. M. Chandrashekar and N. M. Linke, Quantum walks and Dirac cellular automata on a programmable trapped-ion quantum computer, *Nat. Commun.* **11**, 3720 (2020).
- [71] K. A. Landsman, C. Figgatt, T. Schuster, N. M. Linke, B. Yoshida, N. Y. Yao, and C. Monroe, Verified quantum information scrambling, *Nature (London)* **567**, 61 (2019).
- [72] J. Zhang, G. Pagano, P. W. Hess, A. Kyprianidis, P. Becker, H. Kaplan, A. V. Gorshkov, Z.-X. Gong, and C. Monroe, Observation of a many-body dynamical phase transition with a 53-qubit quantum simulator, *Nature (London)* **551**, 601 (2017).
- [73] J. G. Bohnet, B. C. Sawyer, J. W. Britton, M. L. Wall, A. M. Rey, M. Foss-Feig, and J. J. Bollinger, Quantum spin dynamics and entanglement generation with hundreds of trapped ions, *Science* **352**, 1297 (2016).
- [74] Z. Yan, Y.-R. Zhang, M. Gong, Y. Wu, Y. Zheng, S. Li, C. Wang, F. Liang, J. Lin, Y. Xu, C. Guo, L. Sun, X. Peng, K. Xia, H. D. Rong, J. Q. You, F. Nori, H. Fan, X. Zhu, and J. Pan, Strongly correlated quantum walks with a 12-qubit superconducting processor, *Science* **364**, 753 (2019).
- [75] J. A. Smolin and D. P. DiVincenzo, Five two-bit quantum gates are sufficient to implement the quantum Fredkin gate, *Phys. Rev. A* **53**, 2855 (1996).
- [76] M. A. Nielsen and I. L. Chuang, *Quantum Computation and Quantum Information* (Cambridge University Press, Cambridge, 2000).
- [77] A. D. Corcoles, E. Magesan, S. J. Srinivasan, A. W. Cross, M. Steffen, J. M. Gambetta, and J. M. Chow, Demonstration of a quantum error detection code using a square lattice of four superconducting qubits, *Nat. Commun.* **6**, 6979 (2015).
- [78] W. Huggins, P. Patil, B. Mitchell, K. B. Whaley, and E. M. Stoudenmir, Towards quantum machine learning with tensor networks, *Quantum Sci. Technol.* **4**, 2 (2019).